

Article

Effect of Trimethine Cyanine Dye- and Folate-Conjugation on the In Vitro Biological Activity of Proapoptotic Peptides

Davide Cardella ¹, Wenjing Deng ², Louis Y. P. Luk ^{1,*} and Yu-Hsuan Tsai ^{1,2,*} 

¹ School of Chemistry, Main Building, Cardiff University, Park Place, Cardiff CF10 3AT, UK; cardellad@cardiff.ac.uk

² Shenzhen Bay Laboratory, Gaoko Innovation Center, Institute of Molecular Physiology, Guangming District, Shenzhen 518132, China; dengwenjing111@i.smu.edu.cn

* Correspondence: lukly@cardiff.ac.uk (L.Y.P.L.); tsai.y-h@outlook.com (Y.-H.T.)

Abstract: Despite continuous advances, anticancer therapy still faces several technical hurdles, such as selectivity on cellular and subcellular targets of therapeutics. Toward addressing these limitations, we have combined the use of proapoptotic peptides, trimethine cyanine dye, and folate to target the mitochondria of tumor cells. A series of proapoptotic peptides and their conjugates with a cyanine dye and/or folate were synthesized in the solid phase, and their toxicity in different human cell lines was assessed. Cyanine-bearing conjugates were found to be up to 100-fold more cytotoxic than the parent peptides and to localize in mitochondria. However, the addition of a folate motif did not enhance the potency or selectivity of the resulting conjugates toward tumor cells that overexpress folate receptor α . Furthermore, while dual-labeled constructs were also found to localize within the target organelle, they were not generally selective towards folate receptor α -positive cell lines in vitro.

Keywords: cancer; cyanine dyes; folate; mitochondria; proapoptotic peptides; solid-phase synthesis



Citation: Cardella, D.; Deng, W.; Luk, L.Y.P.; Tsai, Y.-H. Effect of Trimethine Cyanine Dye- and Folate-Conjugation on the In Vitro Biological Activity of Proapoptotic Peptides. *Biomolecules* **2022**, *12*, 725. <https://doi.org/10.3390/biom12050725>

Academic Editor: Frank Krause

Received: 7 April 2022

Accepted: 16 May 2022

Published: 20 May 2022

Publisher's Note: MDPI stays neutral with regard to jurisdictional claims in published maps and institutional affiliations.



Copyright: © 2022 by the authors. Licensee MDPI, Basel, Switzerland. This article is an open access article distributed under the terms and conditions of the Creative Commons Attribution (CC BY) license (<https://creativecommons.org/licenses/by/4.0/>).

1. Introduction

Cancer is a leading cause of death worldwide [1]. It is estimated that more than 50% of the people in the UK who are currently under the age of 65 will be diagnosed with cancer during their lifetime [2]. While significant research has been conducted in therapeutic development, the treatment of different cancers still remains an unmet clinical need [3,4]. Thus, there is a necessity for new therapeutic approaches, particularly ones that specifically target cancer cells [5,6]. Such a strategy can maximize potency and minimize off-target side effects of the drugs.

The mitochondrion hosts several putative drug targets of cancer therapy, as the organelle plays key functions in different physiological and pathological cellular processes such as programmed cell death, and hence small-molecule agents that target this organelle are of interest [7]. Many heptamethine cyanine dyes are preferentially localized in the mitochondria of cancer cells and have been employed as imaging probes [8–11]. The mitochondrial targeting ability is believed to be associated with the delocalized lipophilic cationic nature of the dye as depolarization of the mitochondrial membrane prevents accumulation of heptamethine cyanine dyes in mitochondria [12], while selectivity towards cancer cells is thought to be due to the generic negative potential of the cell surface [13]. Moreover, we recently showed that Cy3, a trimethine cyanine dye, can function as a delivery vector selectively targeting mitochondria with a moderate preference toward tumor cells, and its affinity also depends on the mitochondrial membrane potential [14]. It, therefore, is of interest to investigate whether the addition of a cell-targeting component could further improve the cell selectivity of the conjugates.

Folate receptor α , because of its role in uptaking the essential vitamin, is overexpressed in many tumors and hence can be targeted for cargo delivery. To date, many

anti-cancer therapeutics have been preferentially delivered to tumor cells upon conjugation to folate [15–19]. Some of the most successful examples reported in the literature are the conjugation of folate to desacetyl vinblastine monohydrate [20] and taxol derivatives [21]. In both cases, the drug and folate component were separated by a peptidyl spacer and a self-cleaving linker. Additionally, folate conjugation was also proven to be effective in the delivery of antibodies, nanoparticles, and imaging agents [16–18].

Here we tested the hypothesis of whether the covalent addition of folate and cyanine dye will enhance the potency and selectivity of toxic cargoes towards mammalian cells, including cancer cell lines (Figure 1a). Cyanine dye 1 (Figure 1b) and folate were chemically conjugated to the N-terminus of three proapoptotic peptides (2–4) to yield conjugates 5–13 (Table 1). The cytotoxicity of these constructs was evaluated in cancer (i.e., KB, MCF7, and SK-OV-3) and non-cancer (i.e., HEK293) cell lines.

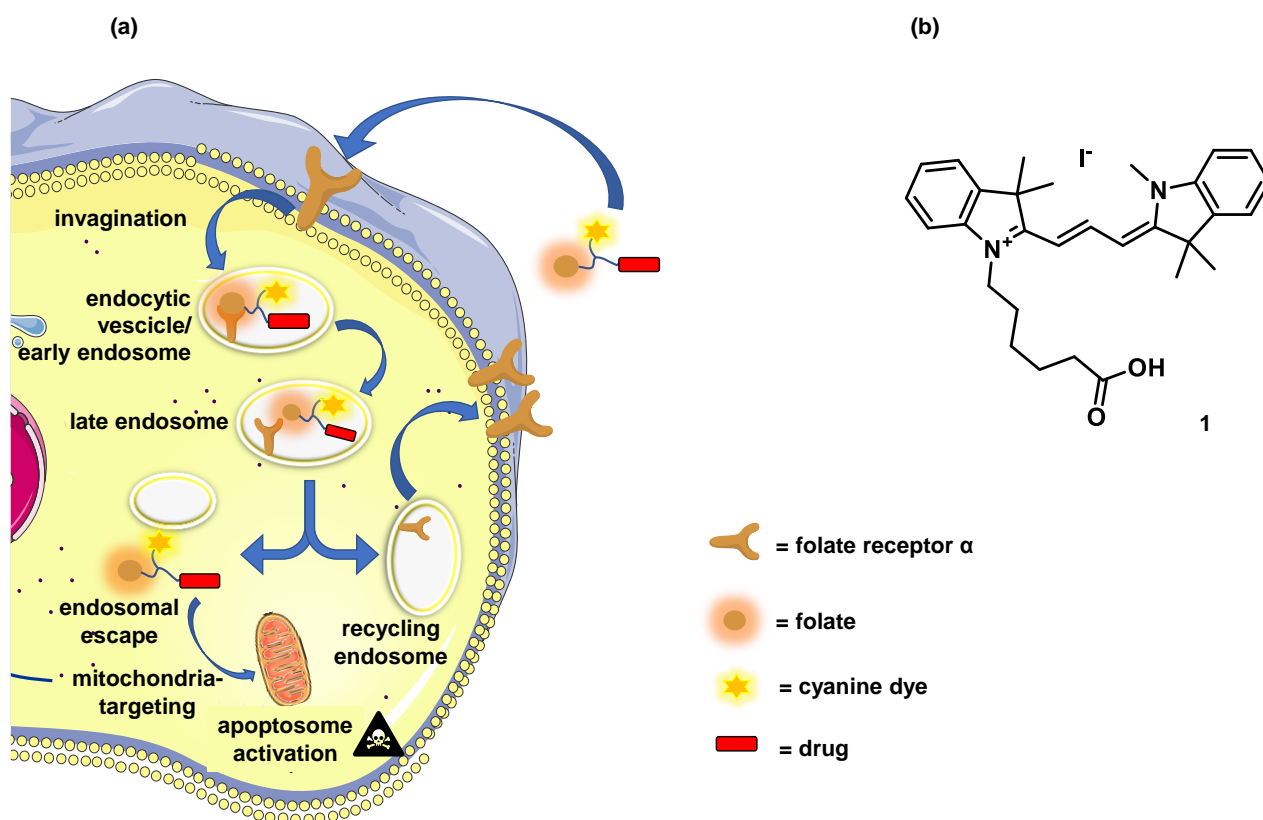
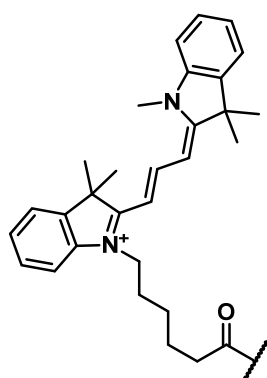
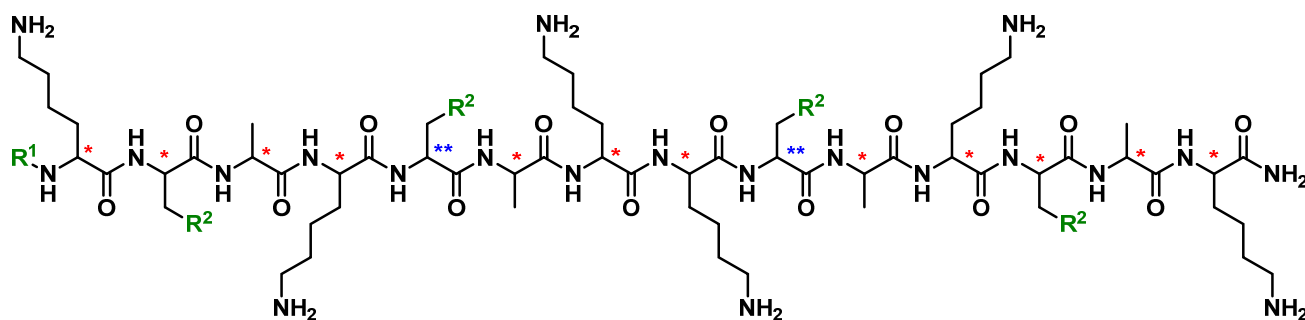
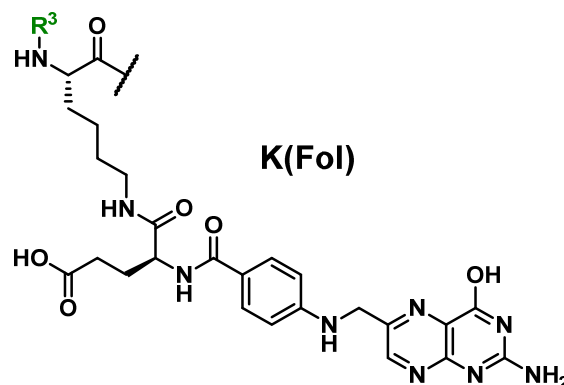


Figure 1. Folate conjugates exploit the folate receptor-mediated endosomal pathways, while the cyanine dye component delivers the construct inside mitochondria. (a) Folate receptor-mediated endocytosis mechanism and cyanine dye-mediated mitochondria-targeting in mammalian cells; (b) Chemical structure of cyanine dye 1.

Table 1. Chemical structure of 2–13 and cytotoxicity values for compounds 1–13. The EC₅₀ values (expressed in μM) on KB, SK-OV-3, MCF7 and HEK293 cells of different molecules and their cyanine dye conjugates were quantified using cell viability assays. Data from three biological replicates were combined and fitted using Origin to obtain the EC₅₀ values and the standard errors (shown in the brackets).



Cy3



K(Fol)

Compound	R ¹	R ²	R ³	*	**	EC ₅₀ in μM			
						KB	SK-OV-3	MCF7	HEK293
1	-	-	-	-	-	36.5 (3.6)	8.6 (6.70)	110 (13.2)	221 (53.8)
2	H	isopropyl	-	(S)	(S)	>400	>400	>400	>400
3	H	isopropyl	-	(R)	(R)	331 (152)	>400	>400	>400
4	H	cyclohexyl	-	(R)	(S)	6.5 (0.5)	11.6 (2.37)	50.9 (3.0)	15.6 (2.6)
5	Cy3	isopropyl	-	(S)	(S)	6.7 (0.2)	11.0 (2.56)	7.37 (0.2)	44.3 (7.0)
6	Cy3	isopropyl	-	(R)	(R)	3.5 (0.1)	6.39 (0.79)	5.7 (0.7)	5.3 (0.2)
7	Cy3	cyclohexyl	-	(R)	(S)	5.5 (0.5)	23.0 (1.64)	11.6 (1.5)	8.2 (0.5)
8	K(Fol)	isopropyl	Cy3	(S)	(S)	38.8 (6.6)	8.8 (3.7)	49.4 (4.3)	35.6 (3.4)
9	K(Fol)	isopropyl	Cy3	(R)	(R)	22.4 (1.4)	8.0 (2.2)	13.2 (5.6)	6.9 (1.8)
10	K(Fol)	cyclohexyl	Cy3	(R)	(S)	3.4 (0.7)	6.0 (1.1)	6.9 (0.9)	6.8 (1.4)
11	K(Fol)	isopropyl	Ac	(S)	(S)	242 (33.2)	>400	>400	>400
12	K(Fol)	isopropyl	Ac	(R)	(R)	151 (38.7)	388.4 (21.3)	>400	>400
13	K(Fol)	cyclohexyl	Ac	(R)	(S)	9.8 (0.6)	41.5 (4.0)	26.9 (7.2)	20.4 (5.7)

* and ** refer to the absolute configuration of the chiral center; Ac = acetyl; pairing anion for compounds 5–7 and 8–10 is assumed to be trifluoroacetate.

2. Materials and Methods

Synthesis of compounds 1–13 is described in the Supplementary Materials.

2.1. Cell Culture

KB and MCF7 cells were kindly gifted by Prof. Arwyn T. Jones (Cardiff University), HEK293 cells were purchased from Public Health England, and SK-OV-3 cells were purchased from National Collection of Authenticated Cell Cultures (<https://cell-bank.org.cn/>). Cells were routinely tested for mycoplasma infection. KB and SK-OV-3 cells were maintained in T75 flasks at 37 °C in a 5% CO₂ atmosphere in folic acid-depleted Roswell Park Memorial Institute (RPMI)-1640 medium supplemented with 10% (*v/v*) fetal bovine serum (FBS). MCF7 and HEK293 cells were maintained in T75 flasks at 37 °C in a 5% CO₂ atmosphere in Dulbecco's Modified Eagle's medium (DMEM) supplemented with 10% (*v/v*) FBS. Cells were maintained at a sub-confluent monolayer and split at 80–85% confluency. For splitting, cells were washed with PBS, trypsinized in 1 mL of trypsin, and 200 µL of the 1000 µL trypsin cell suspension was re-suspended in 12 mL fresh DMEM containing 10% (*v/v*) FBS in a new T75 flask. KB and SK-OV-3 cells were used for biological experiments after being maintained for at least 10 days in folic acid-depleted RPMI-1640 medium.

2.2. Cell Viability Assay

SK-OV-3, MCF7, and HEK293 cells were seeded at a density of 2×10^4 cells per well in a Nunc™ MicroWell™ 96-well plate and grown at 37 °C in a 5% CO₂ atmosphere in DMEM supplemented with 10% (*v/v*) FBS for 24 h. KB cells were seeded at a density of 7×10^3 cells per well in a 96-well plate and grown at 37 °C in a 5% CO₂ atmosphere in folic acid-depleted RPMI-1640 medium supplemented with 10% (*v/v*) FBS for 24 h. Stock solutions of compounds 2–6 and 11–13 were obtained by dissolving the compounds in sterile deionized water. Compounds 1, and 7–10 were dissolved in pure DMSO. The stock solutions were diluted into the proper medium (according to the cell line tested) supplemented with 10% FBS to the appropriate concentration, and cells in each well were incubated with 100 µL of the solution. The solutions in each well were then adjusted to a concentration of 1% (*v/v*) DMSO. After 24 h at 37 °C, 20 µL of CellTiter-Blue™ was added to each well. The plate was incubated for another 4 h at 37 °C before analysis on a Perkin Elmer Victor X plate reader (excitation 531 nm; emission 595 nm). Each data point was calculated from a minimum of nine values resulting from three biological replicates (i.e., cells split from three different passages); each biological replicate is calculated from three technical replicates (i.e., cells split from the same passage). Value from media-only with CellTiter-Blue™ was set at 0% viability. This value was then subtracted from the values from cell-only (i.e., non-treated) wells with CellTiter-Blue™ in each biological replicate and set as 100% viability. For treatments of Cy3-containing compounds, blanks were generated with cell-free wells containing the compounds incubated for 24 h before addition of CellTiter-Blue™. The fluorescent reading for these wells was deducted from the treatment readings. Dose-response fitting curves were generated using Origin, version 2019b, OriginLab Corporation, Northampton, MA, USA (Figures S21–S24, Supplementary Materials).

2.3. Confocal Microscopy

SK-OV-3 and MCF7 were seeded at a density of 1×10^6 cells per well in glass-bottom culture dishes and grown at 37 °C in a 5% CO₂ atmosphere in medium supplemented with 10% (*v/v*) FBS for 24 h. Cells were washed once with the RPMI-1640 medium supplemented with 10% (*v/v*) FBS before staining. Compounds 1, 5–10 were diluted into the RPMI-1640 medium supplemented with 10% (*v/v*) FBS to 10 µM and then added to the culture dishes, respectively. After 10-min incubation at 37 °C, cells were washed with RPMI-1640 medium supplemented with 10% (*v/v*) FBS. Cells were then treated with 50 nM MitoTracker Green FM and 10 µg/mL Hoechst33258 pre-formulated with RPMI-1640 medium supplemented

with 10% (*v/v*) FBS and then incubated for another 10 min at 37 °C before analysis on ZEISS LSM 900 with Airyscan 2. The results were analyzed using Image J software (Figure 3 and Figures S4–S7 in Supplementary Materials).

2.4. Flow Cytometry

SK-OV-3 and MCF7 were seeded at a density of 2×10^5 cells per well in 24-well plate and grown at 37 °C in a 5% CO₂ atmosphere in DMEM medium supplemented with 10% (*v/v*) FBS for 24 h. Cells were washed once with the RPMI-1640 medium supplemented with 10% FBS before staining. Compounds **1**, **5–10** were diluted into the RPMI-1640 medium supplemented with 10% FBS to 10 μM and then added to the culture dishes. After 10-min incubation at 37 °C, cells were washed with RPMI-1640 medium supplemented with 10% FBS. Cells were then treated with 50 nM Mitotracker Green FM and 10 μg/mL Hoechst33258 pre-formulated with RPMI-1640 medium supplemented with 10% FBS for another 10 min at 37 °C. Cells were washed once with PBS before trypsinization for flow cytometry analysis on Invitrogen Attune NxT. The results were analyzed using FlowJo™ v10 Software of BD Life Sciences (Figure S8, Supplementary Materials).

2.5. Statistical Analysis

Comparison of cytotoxicity fitting curves was achieved by applying the extra sum-of-squares F test, performed using GraphPad Prism version 9 for Windows, GraphPad Software, La Jolla, California, USA (<https://www.graphpad.com/>). Statistical difference between cytotoxicity values was assumed when *p*-value, as output of the extra sum-of-squares F test, was found to be below 0.05. Statistical analysis on the flow cytometry data was achieved by applying the unpaired two-tailed *t*-test test, performed using GraphPad Prism version 9 for Windows, GraphPad Software, La Jolla California USA, USA (<https://www.graphpad.com/>).

3. Results

3.1. Synthesis of Peptides and Peptide Conjugates 2–13

Peptides **2–4** were synthesized on a polystyrene-based Rink amide resin using an automated microwave peptide synthesizer. Initial attempts using 2.25 min/coupling yielded both the desired peptide and a truncated side product that lacks an N-terminal lysine residue (Figure S1, Supplementary Materials). This issue was addressed by extending the coupling time (see Supplementary Materials).

The peptidyl backbone of conjugates **5–7** was synthesized following the optimized protocol for the synthesis of peptides **2–4**. After coupling and deprotection of the last amino acid residue, the peptidyl resin was manually coupled to cyanine dye **1**.

For the synthesis of folate-containing conjugates **8–13**, an extra lysine was added at the N-terminal of the peptidyl backbone, and cyanine dye **1** and folate were coupled to its α- and ε-amine groups, respectively. A literature procedure was first attempted [22]. However, this strategy led to folate conjugation at both its α- and γ-carboxylate groups, giving an inseparable mixture of labeled isomers (Figure S2, Supplementary Materials). To overcome this issue, a protected glutamic acid residue, Fmoc-Glu(OtBu)-OH, was first coupled to the peptide, followed by coupling with pteric acid. Since no difference was found in the endocytosis efficiency of conjugates where the folate is labeled through either its α- or γ-carboxylic group [23], we opted for the reaction of the α-carboxylate due to the ready availability of the reagent. As a protecting group for the extra lysine side chain to be conjugated with folate, 4-methyltrityl (Mtt) was chosen for conjugates **8**, **9**, and **11–13**. In this way, the protecting group on the N-terminal lysine could be selectively cleaved with conditions orthogonal to the other protecting groups on the peptidyl resin. However, the synthesis of compound **10** proved to be more challenging. In fact, upon glutamic acid coupling and Fmoc deprotection, the Mtt strategy led to the presence of a peak in the LC-MS chromatogram with a difference of + 129 *m/z* compared to the desired intermediate, attributable to an extra glutamic acid residue (Figure S3, Supplementary Materials). This

is likely due to Boc deprotection during the Mtt cleavage conditions (1% TFA in DCM). Finally, conjugate **10** was obtained using 1-(4,4-dimethyl-2,6-dioxocyclohex-1-ylidene)-3-methylbutyl (ivDde) as a protecting group, which could be cleaved in 4% (*v/v*) hydrazine hydrate in DMF, leading to selective labeling of one folate molecule to the peptide.

3.2. Cytotoxicity of 1–13

Cytotoxicity of **1–13** was evaluated using the CellTiter-Blue assay on KB, MCF7, SK-OV-3, and HEK293 cells. KB cells are derived from human cervical cancer [24], while SK-OV-3 cells are derived from human ovarian cancer. Both cell lines exhibit high levels of folate receptor α on the cell surface [17,25,26]. This feature is of particular relevance in anticancer applications, as it can be exploited for selective targeting and delivery. MCF7 is a cell line derived from human breast cancer with low levels of folate receptor α [27]. Therefore, it can serve as the negative control for folate receptor α mediated tumor-targeted drug delivery systems. HEK293 is a non-cancer cell line and was chosen to evaluate the specificity of the tested compounds toward cancer cells. Cell viability assay results are summarized in Table 1.

Peptides **2** and **3** were found to be the least potent amongst the tested compounds, whereas peptide **4** showed good potency in all tested cell lines. In fact, peptide **4** was designed by engineering the sequence of compounds **2** and **3** via the replacement of the leucine with cyclohexylalanine residues which led to increased cytotoxicity [28]. Cyanine dye-labeled constructs **5–7** were found to be significantly more potent ($p < 0.01$) than the peptides alone (**2–4**) in the tested cell lines—the only exception being the cytotoxicity of compound **7** in KB cells which was not found to be significantly different ($p = 0.11$) to that of its native sequence. Conjugates **11** and **12** bearing a folate component showed enhanced toxicity in KB but not in SK-OV-3 cells when compared to MCF7 and HEK293 cells. Likewise, the cytotoxicity of compound **13** in KB cells was found to be significantly higher ($p < 0.01$) than in the other tested cell lines. Nevertheless, the potency of **11–12** in cells not overexpressing folate receptor α is comparable to that of their native peptides. Lastly, dual labeled conjugates **8–10** showed enhanced potency compared to the parent sequences and to compounds **11–13** ($p < 0.05$), although no selectivity was consistently observed toward KB and SK-OV-3 cells (Figure 2).

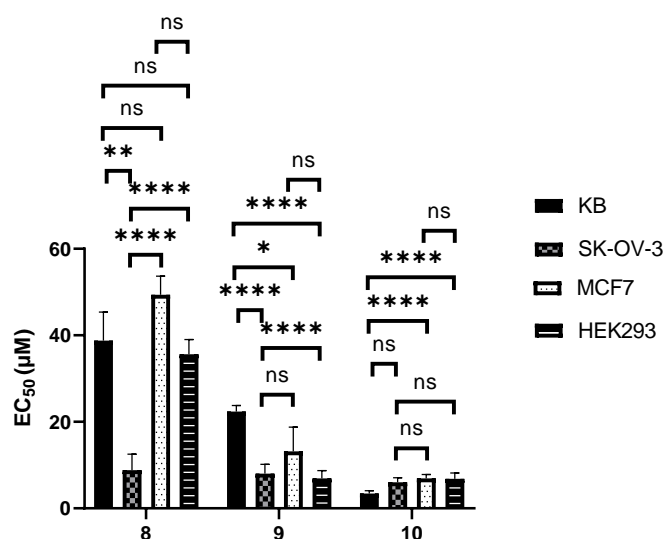


Figure 2. Cytotoxicity of cyanine dye and folate labelled compounds **8–10** in KB, SK-OV-3, MCF7 and HEK293 cells. Bars represent the standard error of the curve fitted using Origin. Statistical analysis was performed by applying the extra sum-of-squares F test, performed using GraphPad Prism version 9 for Windows, GraphPad Software, La Jolla California USA, www.graphpad.com. ns = not statistically significant, * = $p < 0.05$, ** = $p < 0.01$, **** = $p < 0.0001$.

3.3. Mitochondrial Localization and Cellular Uptake of 5–10

To confirm the subcellular localization and uptake of Cy3-containing conjugates, we performed confocal microscopy and flow cytometry analysis of cyanine dye 1 as well as conjugates 5–10 in SK-OV-3 and MCF7 cells. Confocal microscopy results confirmed the mitochondrial localization of 5–10 (Figure 3 and Figures S4–S7 in Supplementary Materials). Flow cytometry analysis showed similar uptake levels of individual conjugates by the two different cell lines (Figure 4 and Figure S8 in Supplementary Materials), but conjugates 8–10 containing both Cy3 and folate were less efficient in entering cells than conjugates 5–7 containing only Cy3. Overall, the less cytotoxic conjugates also have a lower level of cellular uptake.

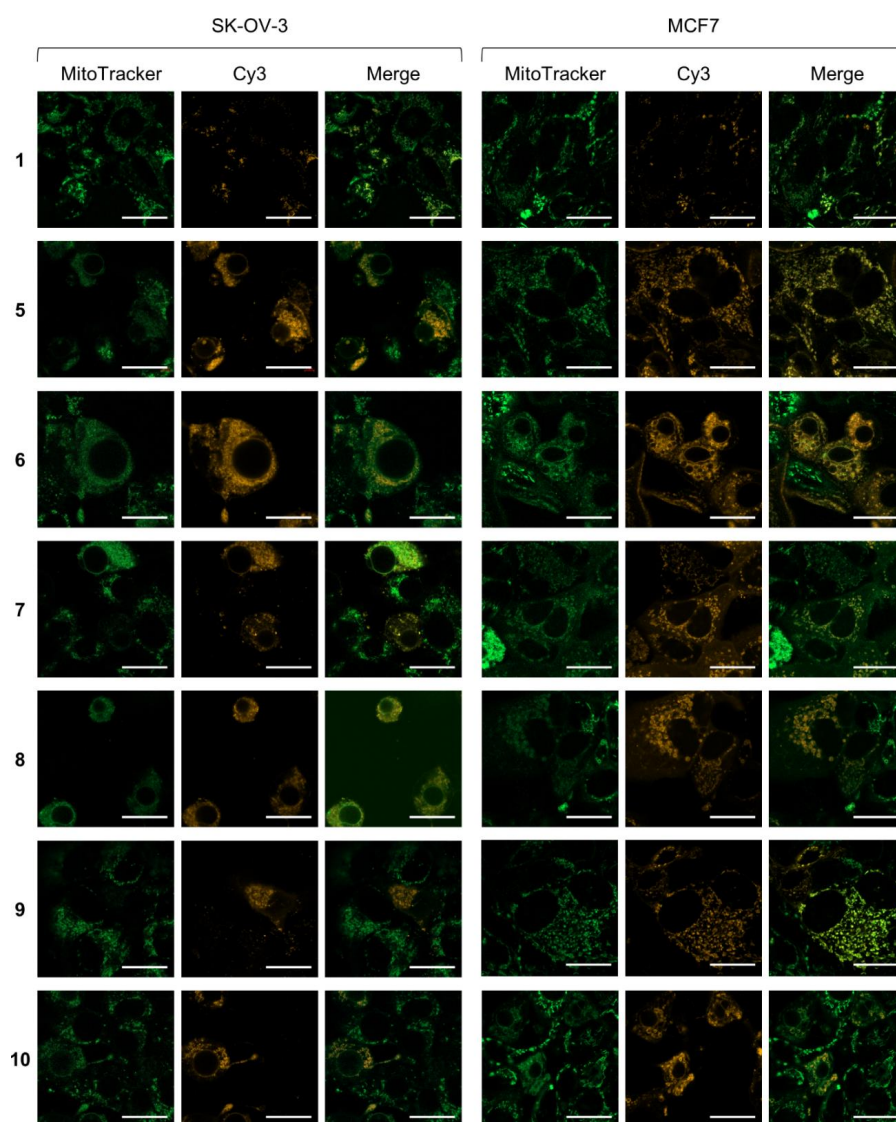


Figure 3. Confocal microscopy images of SK-OV-3 and MCF7 cells treated with Cy3-containing conjugates. Cells were treated with 10 μ M of the indicated conjugate for 10 min at 37 $^{\circ}$ C, washed, stained with 50 nM MitoTracker Green FM and 10 μ g/mL Hoechst33258 for 10 min at 37 $^{\circ}$ C, washed, and imaged at 63X. Pearson's correlation coefficients of MitoTracker Green FM and Cy3 fluorescence for compounds 1, 5, 6, 7, 8, 9, and 10 in SK-OV-3 and MCF7 cells are 0.75/0.64, 0.73/0.81, 0.91/0.61, 0.78/0.63, 0.85/0.69, 0.43/0.82, and 0.78/0.60, respectively. Excitation wavelengths for Hoechst33258, MitoTracker Green FM and Cy3 were set as 405, 488, and 561 nm, respectively. Scale bars denote 25 μ m. Additional images, including the results of Hoechst33258 staining, are shown in Figure S4 (SK-OV-3 at 20X), Figure S5 (SK-OV-3 at 63X), Figure S6 (MCF7 at 20X) and Figure S7 (MCF7 at 63X), Supplementary Materials.

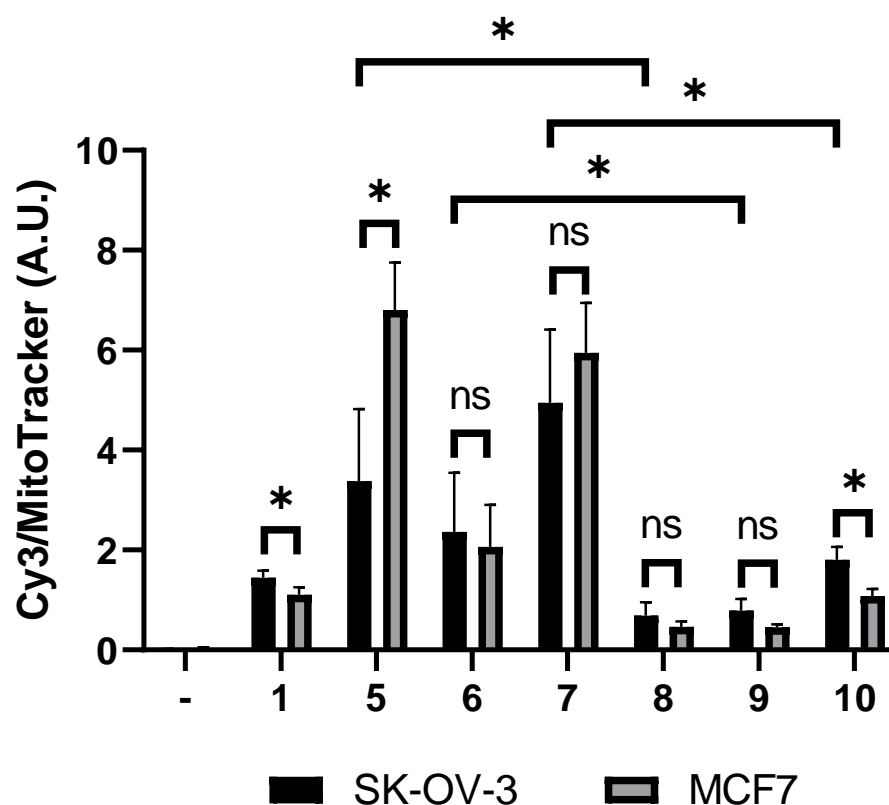


Figure 4. Flow cytometry analysis of Cy3-containing conjugate uptakes by SK-OV-3 and MCF7 cells. Cells were treated with 10 μ M of the indicated conjugate for 10 min at 37 $^{\circ}$ C, washed, stained with 50 nM MitoTracker Green FM for 10 min at 37 $^{\circ}$ C, washed, trypsinized, and subjected to flow cytometry analysis. Cellular uptakes are shown as the ratios of Cy3 and MitoTracker Green FM fluorescence. Mean ratios \pm standard deviations are calculated from three biological replicates and plotted in arbitrary unit (A.U.). The negative control (-) refers to cells only stained with MitoTracker Green FM. Representative flow cytometry scatter plots are shown in Figure S8. Statistical analysis was performed by applying the unpaired two-tailed *t*-test test, performed using GraphPad Prism version 9 for Windows, GraphPad Software, La Jolla California USA, www.graphpad.com. ns = not statistically significant, * = $p < 0.05$.

4. Discussion and Conclusions

Both organelle-specific and receptor-mediated drug delivery systems have proven to be promising tools in anticancer therapy. We have previously shown the efficacy of a trimethine cyanine dye in selectively delivering different cargos to the mitochondria of human cancer cell lines [14]. Many cancer cells overexpress the folate receptor α [17], enabling the use of folate to target cancer cells, especially those derived from ovarian, breast, and lung carcinomas [16]. With these premises, we sought to improve the efficacy of existing proapoptotic peptides 2–4 toward cancer cells via conjugation with both cyanine dye and folate (8–10). For systematic evaluation, conjugates containing either cyanine dye (5–7) or folate (11–13) were also prepared.

The syntheses were accomplished with as little as two equivalents of Fmoc-protected amino acid per coupling, whereas literature procedures for preparing peptides 2 and 3 employed four or more equivalents [22,29]. This is of great relevance when expensive D-amino acid or unnatural amino acid (e.g., cyclohexylalanine) building blocks are used.

Cytotoxicity results obtained by the CellTiter-Blue assay are shown in Table 1. The low activity of peptides 2 and 3 in the tested cell lines ($EC_{50} > 300 \mu$ M) is likely due to their low cell permeability [29–35]. In contrast, peptide 4 was engineered to be more hydrophobic than 2 or 3 by replacing leucine with cyclohexylalanine to improve membrane permeability [28]. Indeed, peptide 4 is significantly more toxic than 2 or 3, and the obtained EC_{50}

values align with the literature [28], confirming the correlation between hydrophobicity and cell permeability [28,36,37]. Interestingly, the EC_{50} value of **4** in MCF7 cells was about 3–8 times higher than in the other tested cell lines.

Delocalized lipophilic cations, such as the triphenylphosphonium group and the cyanine dyes used here, preferentially localize within mitochondria. While the triphenylphosphonium group is widely used to generate mitochondrial-targeting molecules, conjugation of peptide **2** with the triphenylphosphonium group showed negligible toxicity in mammalian cells [22]. In contrast, cyanine dye-labeled constructs **5–7** were generally more potent than the peptides alone (**2–4**) in the tested cell lines. The enhanced potency of these constructs may be due to the increased mitochondrial targeting ability and/or membrane permeability upon conjugation with cyanine dye **1**. Indeed, the confocal microscopy results confirmed the mitochondrial localization of the cyanine dye-labeled constructs (Figure 3).

We were intrigued by the enhanced potency caused by cyanine dye conjugation; we aimed to increase the selectivity of the apoptotic peptides towards cancer cells. Therefore, dual-labeled constructs **8–10** were made with the α -amine of the N-terminal lysine conjugated to cyanine dye **1** and the side chain of the same lysine connected to a folate. As a control, we also prepared and tested the activity of compounds **11–13**, where only folate but not the cyanine dye was included.

To our disappointment, folate-containing constructs (**8–13**) did not display the expected selectivity towards KB and SK-OV-3 cells, regardless of the presence of a cyanine dye motif. Conjugates **11–13** containing only folate but not cyanine dye have comparable potency to the parent sequences **2–4** towards MCF7, SK-OV-3, and HEK293 cells. Similarly, the addition of folate to Cy3-containing conjugates **5–7** has minimal impact on selectivity and potency. Overall, the attachment of a folate motif through its α -carboxylic group to the N-terminus of the peptides did not lead to any notable selectivity towards KB and SK-OV-3. Optimizing the attachment site, linkage, linker, and valency of folate is likely essential for receptor-mediated uptake, conferring tumor cell selectivity.

Previously, attachment of a folate motif to the N-terminus [22,38,39], C-terminus [40], or in the middle of peptides [41] has led to either enhanced selectivity of the construct towards cells overexpressing the folate receptor α or enhanced binding affinity to recombinant folate receptor α . It has been reported that linking the folate via the α - or γ -carboxylic group does not affect the uptake efficiency [23]. However, a different study claimed otherwise [42], and, in most of the successful examples, the folate is connected through its γ -carboxylic group [17]. Many of these constructs also bear a spacer between the folate and the cargo [17]. Although the effects of the linker length and type have not been systematically evaluated, the steric environment around the folate fragment is known to be an important factor in the interaction of the conjugate with the receptor [23]. Besides, some proteins have shown improved uptake by folate receptor α -positive cells when labeled with multiple folate molecules [43,44]. For future work, the attachment site, linkage, linker, and valency of the folate within the constructs will be evaluated.

In conclusion, cyanine dyes are promising tools to further improve the efficacy of drugs in anticancer therapy. Nevertheless, further effort must be made to optimize the design of constructs bearing both components.

Supplementary Materials: The following are available online at <https://www.mdpi.com/article/10.3390/biom12050725/s1>, Chemical synthesis of compounds **1–13**, Figure S1: TIC chromatograms of the crude compound **2**, Figure S2: TIC chromatogram of the crude for the synthesis of compound **8** after coupling folate to the ϵ -amino group of the N-terminal lysine, Figure S3: TIC chromatogram of the crude of synthesis for compound **10** after coupling and deprotection of glutamic acid to the ϵ -amino group of the N-terminal lysine, Figure S4: Confocal microscopy images of SK-OV-3 cells treated with Cy3-containing conjugates at 20X, Figure S5: Confocal microscopy images of SK-OV-3 cells treated with Cy3-containing conjugates at 63X, Figure S6: Confocal microscopy images of MCF7 cells treated with Cy3-containing conjugates at 20X, Figure S7: Confocal microscopy images of MCF7 cells treated with Cy3-containing conjugates at 63X, Figure S8: Representative flow cytometry scatter

plots of Cy3-containing conjugate uptakes by SK-OV-3 and MCF7 cells, Figure S9: TIC chromatogram of compound 2, Figure S10: TIC chromatogram of compound 3, Figure S11: TIC chromatogram of compound 4, Figure S12: TIC chromatogram of compound 5, Figure S13: TIC chromatogram of compound 6, Figure S14: TIC chromatogram of compound 7, Figure S15: TIC chromatogram of compound 8, Figure S16: TIC chromatogram of compound 9, Figure S17: TIC chromatogram of compound 10, Figure S18: TIC chromatogram of compound 11, Figure S19: TIC chromatogram of compound 12, Figure S20: TIC chromatogram of compound 13, Figure S21: Cytotoxicity of compounds 1–13 towards KB cells, Figure S22: Cytotoxicity of compounds 1–13 towards MCF7 cells, Figure S23: Cytotoxicity of compounds 1–13 towards HEK293 cells, Figure S24: Cytotoxicity of compounds 1–13 towards SK-OV-3 cells, Table S1: Calculated and found mass to charge ratio for compounds 1–13 by mass spectroscopy. Reference [45] are cited in supplementary materials.

Author Contributions: D.C. performed the synthesis and the characterization. D.C. and W.D. performed the biological experiments. D.C., L.Y.P.L., and Y.-H.T. designed the overall study. D.C. wrote the manuscript. L.Y.P.L. and Y.-H.T. edited the manuscript. All authors have read and agreed to the published version of the manuscript.

Funding: This research was funded by Welsh Government through a Life Sciences Research Network Wales Scholarship to D.C. The APC was funded by UK Research and Innovation.

Institutional Review Board Statement: Not applicable.

Informed Consent Statement: Not applicable.

Acknowledgments: We thank Arwyn T. Jones for the donation of MCF7 cell lines, Alexander R. Nödling and Xuefei Li for the help in the organic lab, Emily M. Mills for the help in the cell culture lab, Yang Huang and Yuanshan Luo for data acquisition, Kung Ching Cookson Chiu of the SZBL Mass Spectrometry Facility for assistance and Victoria L. Barlow for language editing and proofreading the manuscript.

Conflicts of Interest: The authors declare no conflict of interest.

References

1. Wang, H.; Naghavi, M.; Allen, C.; Barber, R.M.; Bhutta, Z.A.; Carter, A.; Casey, D.C.; Charlson, F.J.; Chen, A.Z.; Coates, M.M.; et al. Global, regional, and national life expectancy, all-cause mortality, and cause-specific mortality for 249 causes of death, 1980–2015: A systematic analysis for the Global Burden of Disease Study 2015. *Lancet* **2016**, *388*, 1459–1544. [[CrossRef](#)]
2. Torre, L.A.; Siegel, R.L.; Ward, E.M.; Jemal, A. Global Cancer Incidence and Mortality Rates and Trends—An Update. *Cancer Epidemiol. Biomark. Prev.* **2016**, *25*, 16–27. [[CrossRef](#)] [[PubMed](#)]
3. Ahmad, A.S.; Ormiston-Smith, N.; Sasieni, P.D. Trends in the lifetime risk of developing cancer in Great Britain: Comparison of risk for those born from 1930 to 1960. *Br. J. Cancer* **2015**, *112*, 943–947. [[CrossRef](#)] [[PubMed](#)]
4. Pucci, C.; Martinelli, C.; Ciofani, G. Innovative approaches for cancer treatment: Current perspectives and new challenges. *Ecancermedicalscience* **2019**, *13*, 961. [[CrossRef](#)]
5. Dagogo-Jack, I.; Shaw, A.T. Tumour heterogeneity and resistance to cancer therapies. *Nat. Rev. Clin. Oncol.* **2018**, *15*, 81–94. [[CrossRef](#)] [[PubMed](#)]
6. Langer, R. Drugs on Target. *Science* **2001**, *293*, 58. [[CrossRef](#)]
7. Roth, K.G.; Mambetsariev, I.; Kulkarni, P.; Salgia, R. The Mitochondrion as an Emerging Therapeutic Target in Cancer. *Trends Mol. Med.* **2020**, *26*, 119–134. [[CrossRef](#)]
8. Usama, S.M.; Park, G.K.; Nomura, S.; Baek, Y.; Choi, H.S.; Burgess, K. Role of Albumin in Accumulation and Persistence of Tumor-Seeking Cyanine Dyes. *Bioconj. Chem.* **2020**, *31*, 248–259. [[CrossRef](#)]
9. Yang, X.; Shi, C.; Tong, R.; Qian, W.; Zhau, H.E.; Wang, R.; Zhu, G.; Cheng, J.; Yang, V.W.; Cheng, T.; et al. Near IR heptamethine cyanine dye-mediated cancer imaging. *Clin. Cancer Res.* **2010**, *16*, 2833–2844. [[CrossRef](#)]
10. Jiang, Z.; Pflug, K.; Usama, S.M.; Kuai, D.; Yan, X.; Sitcheran, R.; Burgess, K. Cyanine–Gemcitabine Conjugates as Targeted Theranostic Agents for Glioblastoma Tumor Cells. *J. Med. Chem.* **2019**, *62*, 9236–9245. [[CrossRef](#)]
11. Liu, Y.; Zhou, J.; Wang, L.; Hu, X.; Liu, X.; Liu, M.; Cao, Z.; Shangguan, D.; Tan, W. A Cyanine Dye to Probe Mitophagy: Simultaneous Detection of Mitochondria and Autolysosomes in Live Cells. *J. Am. Chem. Soc.* **2016**, *138*, 12368–12374. [[CrossRef](#)] [[PubMed](#)]
12. Onoe, S.; Temma, T.; Shimizu, Y.; Ono, M.; Saji, H. Investigation of cyanine dyes for in vivo optical imaging of altered mitochondrial membrane potential in tumors. *Cancer Med.* **2014**, *3*, 775–786. [[CrossRef](#)] [[PubMed](#)]
13. Zhang, B.-B.; Liu, J.-g.; Bai, X.-Y.; Huang, Y.-J.; Xu, N.; Ren, T. A Novel Fluorescent Dye Invades Mitochondria to Selectively Kill Cancer Stem Cells via Increased ROS Production. *Bioinorg. Chem. Appl.* **2021**, *2021*, 4763944. [[CrossRef](#)] [[PubMed](#)]

14. Nödling, A.R.; Mills, E.M.; Li, X.; Cardella, D.; Sayers, E.J.; Wu, S.-H.; Jones, A.T.; Luk, L.Y.P.; Tsai, Y.-H. Cyanine dye mediated mitochondrial targeting enhances the anti-cancer activity of small-molecule cargoes. *Chem. Commun.* **2020**, *56*, 4672–4675. [[CrossRef](#)]
15. Leamon, C.P.; Pastan, I.; Low, P.S. Cytotoxicity of folate-Pseudomonas exotoxin conjugates toward tumor cells. Contribution of translocation domain. *J. Biol. Chem.* **1993**, *268*, 24847–24854. [[CrossRef](#)]
16. Cheung, A.; Bax, H.J.; Josephs, D.H.; Ilieva, K.M.; Pellizzari, G.; Opzoomer, J.; Bloomfield, J.; Fittall, M.; Grigoriadis, A.; Figini, M.; et al. Targeting folate receptor alpha for cancer treatment. *Oncotarget* **2016**, *7*, 52553–52574. [[CrossRef](#)]
17. Fernández, M.; Javaid, F.; Chudasama, V. Advances in targeting the folate receptor in the treatment/imaging of cancers. *Chem. Sci.* **2018**, *9*, 790–810. [[CrossRef](#)]
18. Sudimack, J.; Lee, R.J. Targeted drug delivery via the folate receptor. *Adv. Drug Del. Rev.* **2000**, *41*, 147–162. [[CrossRef](#)]
19. Vlahov, I.R.; Leamon, C.P. Engineering Folate–Drug Conjugates to Target Cancer: From Chemistry to Clinic. *Bioconj. Chem.* **2012**, *23*, 1357–1369. [[CrossRef](#)]
20. Leamon, C.P.; Vlahov, I.R.; Reddy, J.A.; Vetzal, M.; Santhapuram, H.K.R.; You, F.; Bloomfield, A.; Dorton, R.; Nelson, M.; Kleindl, P.; et al. Folate–Vinca Alkaloid Conjugates for Cancer Therapy: A Structure–Activity Relationship. *Bioconj. Chem.* **2014**, *25*, 560–568. [[CrossRef](#)]
21. Seitz, J.D.; Vineberg, J.G.; Herlihy, E.; Park, B.; Melief, E.; Ojima, I. Design, synthesis and biological evaluation of a highly-potent and cancer cell selective folate–taxoid conjugate. *Biorg. Med. Chem.* **2015**, *23*, 2187–2194. [[CrossRef](#)] [[PubMed](#)]
22. Vergel Galeano, C.F.; Rivera Monroy, Z.J.; Rosas Pérez, J.E.; García Castañeda, J.E. Efficient Synthesis of Peptides with 4-Methylpiperidine as Fmoc Removal Reagent by Solid Phase Synthesis. *J. Mex. Chem. Soc.* **2014**, *58*, 386–392. [[CrossRef](#)]
23. Chen, W.-H.; Xu, X.-D.; Luo, G.-F.; Jia, H.-Z.; Lei, Q.; Cheng, S.-X.; Zhuo, R.-X.; Zhang, X.-Z. Dual-Targeting Pro-apoptotic Peptide for Programmed Cancer Cell Death via Specific Mitochondria Damage. *Sci. Rep.* **2013**, *3*, 3468. [[CrossRef](#)] [[PubMed](#)]
24. Leamon, C.P.; Deprince, R.B.; Hendren, R.W. Folate-mediated Drug Delivery: Effect of Alternative Conjugation Chemistry. *J. Drug Target.* **1999**, *7*, 157–169. [[CrossRef](#)] [[PubMed](#)]
25. Vaughan, L.; Glänzel, W.; Korch, C.; Capes-Davis, A. Widespread Use of Misidentified Cell Line KB (HeLa): Incorrect Attribution and Its Impact Revealed through Mining the Scientific Literature. *Cancer Res.* **2017**, *77*, 2784–2788. [[CrossRef](#)]
26. Zhang, L.; Hou, S.; Mao, S.; Wei, D.; Song, X.; Lu, Y. Uptake of folate-conjugated albumin nanoparticles to the SKOV3 cells. *Int. J. Pharm.* **2004**, *287*, 155–162. [[CrossRef](#)] [[PubMed](#)]
27. Xing, L.; Xu, Y.; Sun, K.; Wang, H.; Zhang, F.; Zhou, Z.; Zhang, J.; Zhang, F.; Caliskan, B.; Qiu, Z.; et al. Identification of a peptide for folate receptor alpha by phage display and its tumor targeting activity in ovary cancer xenograft. *Sci. Rep.* **2018**, *8*, 8426. [[CrossRef](#)]
28. Elwood, P.C. Molecular cloning and characterization of the human folate-binding protein cDNA from placenta and malignant tissue culture (KB) cells. *J. Biol. Chem.* **1989**, *264*, 14893–14901. [[CrossRef](#)]
29. Horton, K.L.; Kelley, S.O. Engineered Apoptosis-Inducing Peptides with Enhanced Mitochondrial Localization and Potency. *J. Med. Chem.* **2009**, *52*, 3293–3299. [[CrossRef](#)]
30. Law, B.; Quinti, L.; Choi, Y.; Weissleder, R.; Tung, C.H. A mitochondrial targeted fusion peptide exhibits remarkable cytotoxicity. *Mol. Cancer Ther.* **2006**, *5*, 1944–1949. [[CrossRef](#)]
31. Ellerby, H.M.; Arap, W.; Ellerby, L.M.; Kain, R.; Andrusiak, R.; Rio, G.D.; Krajewski, S.; Lombardo, C.R.; Rao, R.; Ruoslahti, E.; et al. Anti-cancer activity of targeted pro-apoptotic peptides. *Nat. Med.* **1999**, *5*, 1032–1038. [[CrossRef](#)] [[PubMed](#)]
32. Jung, H.K.; Kim, S.; Park, R.W.; Park, J.Y.; Kim, I.S.; Lee, B. Bladder tumor-targeted delivery of pro-apoptotic peptide for cancer therapy. *J. Control. Release* **2016**, *235*, 259–267. [[CrossRef](#)] [[PubMed](#)]
33. Qiao, Z.-Y.; Lai, W.-J.; Lin, Y.-X.; Li, D.; Nan, X.-H.; Wang, Y.; Wang, H.; Fang, Q.-J. Polymer–KLAK Peptide Conjugates Induce Cancer Cell Death through Synergistic Effects of Mitochondria Damage and Autophagy Blockage. *Bioconj. Chem.* **2017**, *28*, 1709–1721. [[CrossRef](#)] [[PubMed](#)]
34. Smolarczyk, R.; Cichoń, T.; Graja, K.; Hucz, J.; Sochanik, A.; Szala, S. Antitumor effect of RGD-4C-GG-D(KLAKLAK)₂ peptide in mouse B16(F10) melanoma model. *Acta Biochim. Pol.* **2006**, *53*, 801–805. [[CrossRef](#)] [[PubMed](#)]
35. Mai, J.C.; Mi, Z.; Kim, S.H.; Ng, B.; Robbins, P.D. A proapoptotic peptide for the treatment of solid tumors. *Cancer Res.* **2001**, *61*, 7709–7712.
36. Kim, H.Y.; Kim, S.; Youn, H.; Chung, J.-K.; Shin, D.H.; Lee, K. The cell penetrating ability of the proapoptotic peptide, KLAK-LAKKLAKLAK fused to the N-terminal protein transduction domain of translationally controlled tumor protein, MIIYRDLISH. *Biomaterials* **2011**, *32*, 5262–5268. [[CrossRef](#)]
37. Horton, K.L.; Stewart, K.M.; Fonseca, S.B.; Guo, Q.; Kelley, S.O. Mitochondria-penetrating peptides. *ACS Chem. Biol.* **2008**, *15*, 375–382. [[CrossRef](#)]
38. Horton, K.L.; Pereira, M.P.; Stewart, K.M.; Fonseca, S.B.; Kelley, S.O. Tuning the activity of mitochondria-penetrating peptides for delivery or disruption. *ChemBioChem* **2012**, *13*, 476–485. [[CrossRef](#)]
39. Marverti, G.; Marraccini, C.; Martello, A.; D’Arca, D.; Pacifico, S.; Guerrini, R.; Spyrakis, F.; Gozzi, G.; Lauriola, A.; Santucci, M.; et al. Folic Acid–Peptide Conjugates Combine Selective Cancer Cell Internalization with Thymidylate Synthase Dimer Interface Targeting. *J. Med. Chem.* **2021**, *64*, 3204–3221. [[CrossRef](#)]

40. Kim, W.H.; Kim, C.G.; Kim, M.H.; Kim, D.-W.; Park, C.R.; Park, J.Y.; Lee, Y.-S.; Youn, H.; Kang, K.W.; Jeong, J.M.; et al. Preclinical evaluation of isostructural Tc-99m- and Re-188-folate-Gly-Gly-Cys-Glu for folate receptor-positive tumor targeting. *Ann. Nucl. Med.* **2016**, *30*, 369–379. [[CrossRef](#)]
41. Leamon, C.P.; Reddy, J.A.; Vlahov, I.R.; Westrick, E.; Dawson, A.; Dorton, R.; Vetzal, M.; Santhapuram, H.K.; Wang, Y. Preclinical Antitumor Activity of a Novel Folate-Targeted Dual Drug Conjugate. *Mol. Pharm.* **2007**, *4*, 659–667. [[CrossRef](#)] [[PubMed](#)]
42. Dharmatti, R.; Miyatake, H.; Nandakumar, A.; Ueda, M.; Kobayashi, K.; Kiga, D.; Yamamura, M.; Ito, Y. Enhancement of Binding Affinity of Folate to Its Receptor by Peptide Conjugation. *Int. J. Mol. Sci.* **2019**, *20*, 2152. [[CrossRef](#)] [[PubMed](#)]
43. Wang, S.; Low, P.S. Folate-mediated targeting of antineoplastic drugs, imaging agents, and nucleic acids to cancer cells. *J. Control. Release* **1998**, *53*, 39–48. [[CrossRef](#)]
44. Leamon, C.P.; Low, P.S. Delivery of macromolecules into living cells: A method that exploits folate receptor endocytosis. *Proc. Natl. Acad. Sci. USA* **1991**, *88*, 5572–5576. [[CrossRef](#)]
45. Kvach, M.V.; Ustinov, A.V.; Stepanova, I.A.; Malakhov, A.D.; Skorobogatyi, M.V.; Shmanai, V.V.; Korshun, V.A. A Convenient Synthesis of Cyanine Dyes: Reagents for the Labeling of Biomolecules. *Eur. J. Org. Chem.* **2008**, *2008*, 2107–2117. [[CrossRef](#)]